Lawrence Berkeley National Laboratory

Title
Study of bulk properties at high energy nuclear collisions - The search for the partonic equation of state at RHIC

Permalink
https://escholarship.org/uc/item/0ns2b142

Author
Xu, Nu

Publication Date
2004

Peer reviewed

Study of Bulk Properties at High Energy Nuclear Collisions
– The search for the partonic equation of state at RHIC

Nu Xu

Nuclear Science Division

Lawrence Berkeley National Laboratory, Berkeley, CA 94720, USA

We discuss recent results from RHIC. Issues of energy loss and partonic collectivity from $Au + Au$ collisions at $\sqrt{s_{\mathrm{NN}}} = 200$ GeV are the focus of this paper. We propose a path toward the understanding of the partonic Equation of State in high energy nuclear collisions.

1. Introduction

The purpose of the heavy ion program at Brookhaven National Laboratory is to probe strongly interacting matter under extreme conditions, *i.e.* at high densities and temperatures. Naturally the search for the existence of a new form of matter - the quark-gluon plasma (QGP) - is the experimental focus of the program.

Lattice QCD calculations [1,2] predict the transition between QGP and hadronic state at $T_c \approx 150 - 180$ MeV with vanishing baryon density[1]. The energy density at the transition point is determined to be $\epsilon_c \approx 0.7 - 1.0$ GeV/fm^3. Under the same condition, chiral symmetry restoration also happens [1]. Therefore experimentally one would search for signatures of both QGP formation and in-medium effects of hadron properties.

In high energy nuclear collisions, the term flow has two important aspects: (i) collectivity of produced hadrons and (ii) the local thermalization among these hadron [3]. As long as there are interactions among constituents, collectivity of the matter will be developed provided there is inhomogeneity of matter density. When the interactions last long enough the system will approach local equilibrium and hence develop flow. At the early stage of the collision, both density of the matter and gradient are large, therefore we expect the development of partonic collectivity - the collective motion of partons. The issues of thermalization can be addressed by studying heavy-flavor ($c-, b-$ quarks) collectivity, because the collisions that generate the collective motion for heavy-quarks will likely lead to thermalization among the light quarks ($u-, d-, s-$ quarks). It is important to note that collectivity is cumulative and it is not affected by the details of the hadronization process.

Many exciting results emerged from the RHIC experiments since its first started in the year of 2000. Using high transverse momentum hadrons we demonstrated the interactions at early stage of the collisions. These interactions are most likely to occur among the

---

[1]Including finite baryon density does not affect general properties of the phase transition in Lattice results [4]

partons. At RHIC, much stronger collective flow has been observed, especially for the early developing v_2, compared to results from lower energy heavy ion collisions. This might imply that rescattering effects arise from the partonic stage at RHIC.

This report will summarize the recent results from experiments at RHIC. It will be divided into three parts: (i) observations at the intermediate transverse momentum region ($3 \leq p_T \leq 10$ GeV/c); (ii) bulk properties of the matter produced at RHIC; (iii) evidence of partonic collectivity at RHIC. Finally, the report will be ended with a brief summary and outlook.

2. Energy loss – Interactions at early partonic stage

The measurements of hadron yields at intermediate transverse momentum region ($2 \leq p_T \leq 10$ GeV/c) have demonstrated that hot and dense is matter produced in Au+Au collisions at RHIC [5–7]. Nuclear effects on the inclusive spectra are measured by comparison to a nucleon-nucleon (NN) reference via the nuclear modification factor[2]

$$R_{AB}(p_T) = \frac{d^2 N^{AB}/dp_T d\eta}{T_{AB} d^2 \sigma^{pp}/dp_T d\eta} \tag{1}$$

where $T_{AB} = \langle N_{bin} \rangle / \sigma_{inel}^{NN}$ from a Glauber calculation accounts for the nuclear collision geometry. The spectrum from the non-single-diffractive (NSD) $p + p$ interactions was used. Figure 1 shows $R_{AA}(p_T)$ at $\sqrt{s_{NN}} = 200$ GeV for centrality selected $Au + Au$ spectra relative to the measured $p + p$ spectrum. Horizontal hatched bands show Glauber model expectations for scaling of the yield with $\langle N_{bin} \rangle$ (right side, lightly shaded) or mean number of participants $\langle N_{part} \rangle$ (left side, darkly shaded) and the widths showing their respective uncertainties. It is evident that hadron production for $6 \leq p_T \leq 10$ GeV/c is suppressed by a factor 4-5 in central $Au + Au$ collisions relative to $p + p$ collisions. The apparent suppression decreases monotonically from central to peripheral $Au + Au$ collisions. Compared with $p + p$ collisions, the spectrum from central $Au + Au$ collisions is modified presumably due to rescatterings of energetic particles in the hot and dense medium.

---

[2]The nuclear modification factor can also be extracted from the ratio of R_{CP} (central over peripheral collisions):

$$R_{CP}(p_T) = \frac{[dN/(N_{bin} dp_T]^{Central}}{[dN/(N_{bin} dp_T]^{Peripheral}}$$

where $R_{CP} \sim 1$ if particle production is equivalent to a superposition of independent nucleon-nucleon collisions. Except the nuclear collision geometry, both R_{CP} and R_{AB} represent the same physics.
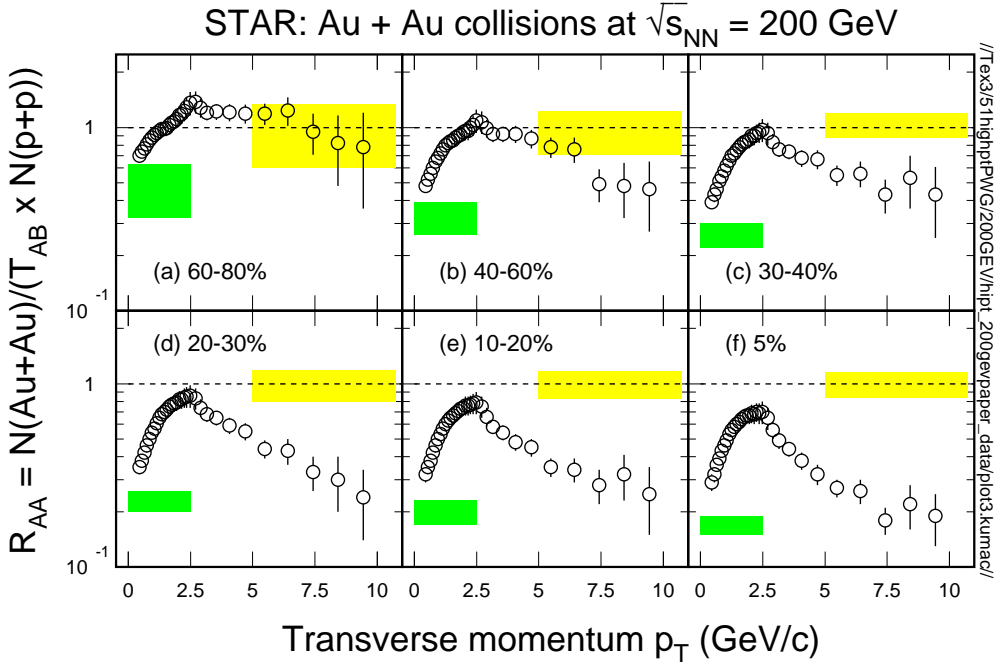
Figure 1 *Mid-rapidity charged hadron $R_{AA}(p_T)$ in ($|\eta| \le 0.5$), for centrality selected $Au+Au$ spectra relative to the measured $p+p$ spectrum. The $p+p$ spectrum is common to all panels. The left hatched bands denote the uncertainties in determining the number of participants, the right hatched bands indicate the uncertainties in determining the number of binary collisions.*

Note that the basic idea behind the nuclear modification factor R_{AB} is to normalize the transverse momentum distribution from nuclear collisions to that of from elementary $p + p$ collisions [8,9]. The normalization is done with the assumption of binary collision $\langle N_{bin} \rangle$ scaling in hard collisions:

$$\sigma_{pA} = \sigma_{NN} \times A^{\alpha}, \tag{2}$$

with $\alpha = 1$. However, up to $p_T \sim 10$ GeV/c, the scaling is violated in hadron productions in all $p + A$ collisions [10,11]. The exceptions are the Drell-Yan processes and direct photon production [10,12]. This indicates that the observed p_T broadening effect in proton induced interactions is, at least partly in my view, due to final state interactions, *i.e.*, the interaction among the produced particles. Since heavy flavors are created at the early stage of the collision, a comparison of the R_{AB} results from both $Au+Au$ and $d+Au$ collisions will shed light on this problem.

When normalized to the corresponding number of binary collisions, the hadron productions at intermediate p_T in ultra-relativistic interactions of heavy nuclei reveal a clear suppression of both the single-particle inclusive yields [5,6,13–15] and back-to-back pairs [16,17] in the most central $Au+Au$ collisions (5%) (see Figures 1 and 2). There are three possible explanations:

1. **Initial Condition:** In this hypothesis, the suppression results from initial-state effects prior to the hard scattering, such as the saturation of gluon density in the

incoming nuclei [18]. Subsequent interactions merely materialize the hadrons from the intrinsic parton distributions.

2. **Parton Energy Loss:** Energetic partons created via hard scatterings traverse the hot and dense medium and loss their energy. The observed highly correlated high p_T hadrons are primarily those created from partons produced near the surface and directed outwards. In this scenario, the interactions take place at the parton stage and the effect is refereed as "jet-quenching" [19].

3. **Hadron Energy Loss:** Qualitatively, due to in medium scatterings among hadrons, the fragmented hadrons should also suffer energy loss, as discussed in Ref. [20]. An energetic parton often leads a cluster of highly correlated hadrons, therefore, one might expect different pattern in the suppression and azimuthal distributions between partonic and hadronic energy loss.
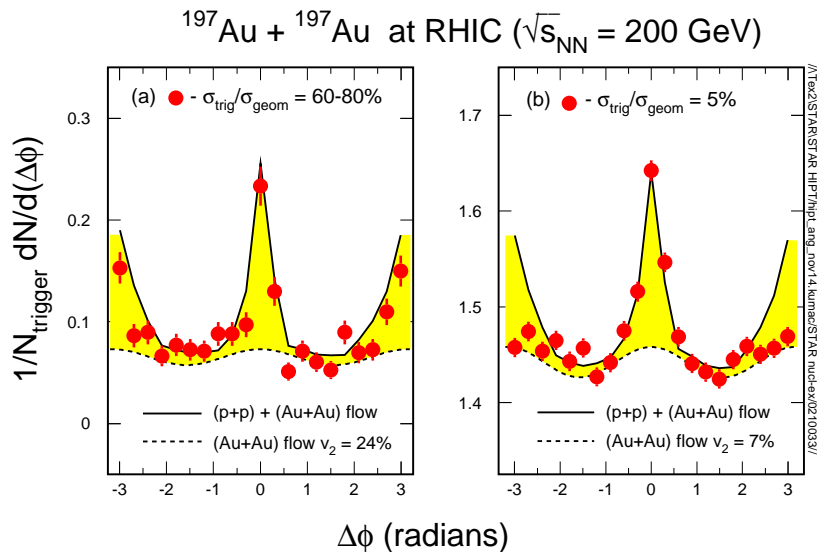

Figure 2 *Mid-rapidity azimuthal distributions from peripheral (left-plot) and central (right-plot) Au + Au collisions at 200 GeV. The dashed-lines represent the anisotropy distributions (often called elliptic flow) from low p_T hadrons at corresponding collision centrality. The solid-lines are the sum of the azimuthal distributions from $p + p$ and flow. The back-to-back hadrons are clearly suppressed in central collisions.*

In order to discriminate between initial condition and final state interaction induced parton energy loss, the study of $d + Au$ collisions were performed. The STAR results [7] are sketched in Figure 3: Left: R_{AB} for central d+Au (20%) and central $Au + Au$ (5%) collisions at $\sqrt{s_{\mathrm{NN}}} = 200$ GeV; Right: Comparison of two-particle azimuthal distributions for central $d + Au$ (20%) collisions to the minimum bias $p + p$ and central $Au + Au$ (5%) collisions.

The nuclear modification factor R_{AB} clearly shows the drastic difference between central $d + Au$ and $Au + Au$ collisions and the same is for the azimuthal distributions. In fact, the azimuthal distributions in $d + Au$ collisions are similar to those of $p + p$ collisions. The R_{AB} results from all RHIC experiments are consistent [21–23].

The fact that no suppression in hadron yields from $d + Au$ collisions for $2 \leq p_T \leq 7$ GeV/c is seen and the two-particle azimuthal distribution in $p + p$ and $d + Au$ collisions are similar suggests that the suppression observed in central $Au + Au$ collisions is due to the final-state interactions. Here the term final-state interaction referees to the reactions among the produced particles, either partons with partons or hadrons with hadrons, or both. It remains an open issue whether the partonic or hadronic interactions dominate such processes that lead to the observed suppression. However, during the early stage of high energy nuclear collisions both particle density and energy density are high, and the wave-functions of particles are overlapping, one might wonder whether the concept of hadronic interactions at such stage is meaningful.
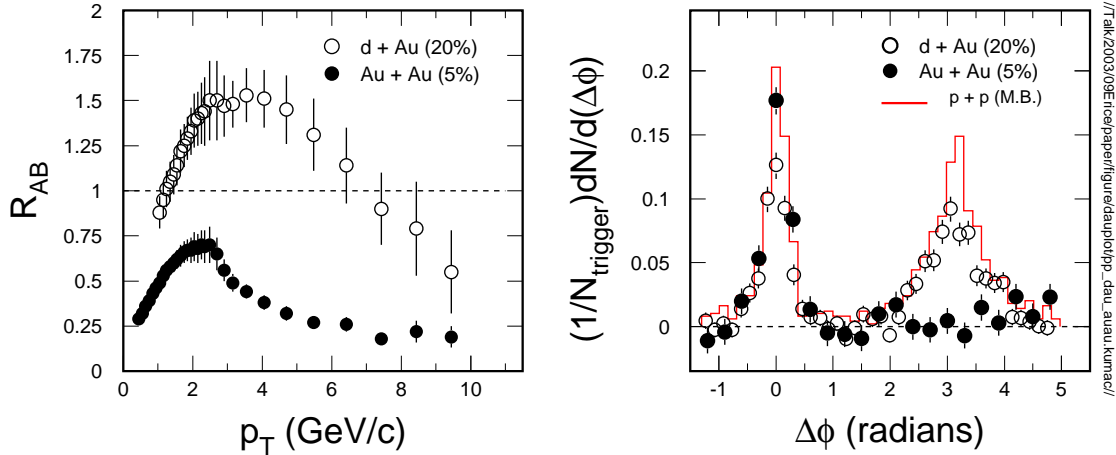

Figure 3 Left: R_{AB} *for central d+Au (20%) and central $Au + Au$ (5%) collisions at* $\sqrt{s_{\mathrm{NN}}} = 200$ *GeV;* **Right:** *Comparison of two-particle azimuthal distributions for central* $d + Au$ *(20%) collisions to the minimum bias $p + p$ and central $Au + Au$ (5%) collisions.*

Figure 4 shows the STAR preliminary results [24–26] of mid-rapidity R_{CP} for mesons (a) and baryons (b), using the top 5% central collisions normalized by the 40-60% peripheral collisions. For most of the intermediate p_T region, R_{CP} for baryons is similar to expectations of N_{bin} scaling and $R_{CP}^{meson} \leq R_{CP}^{baryon}$. At higher p_T ($p_T \geq 5$ GeV/c), the values of R_{CP} begin to decrease and merge together with that of charged hadrons.

The particle type dependence of R_{CP} at intermediate p_T is in contradiction with the expectations from energy loss followed by fragmentation in vacuum. The enhancement of yield at intermediate p_T in proton induced collisions, *i.e.* the Cronin effect [27], has been observed at all collision energies with a larger effect of the enhancement for protons than for mesons [28]. The Cronin effect has been attributed to initial-state rescattering. The strong particle-type dependence of the effect indicates a medium modification to the parton fragmentation: the final hadron spectrum is affected by both the type of the hadron and the medium. In $p + p$ or $p + A$ collision, parton fragmentation dominates the hadronization process. The suppression and the particle-type dependence of R_{CP} (see Figure 4) may reflect bulk partonic matter hadronization in heavy ion collisions.

It is obvious that the description of the energy loss of a jet or a fast moving hadron in the hot and dense medium is only possible from a microscopic point of view. The energetic

object (parton or hadron) is viewed as a microscopic probe. In deed, the pQCD inspired model calculations are all constructed with the concept[19,29]. The approaches bared on coherence effects [18] appear not to work at least for mid-rapidity at RHIC. However, because the system created in $Au + Au$ collisions is large, hot and dense, collective motion at the macroscopic level must exist. In the following sections, we will discuss collective behavior observed in high energy nuclear collisions.
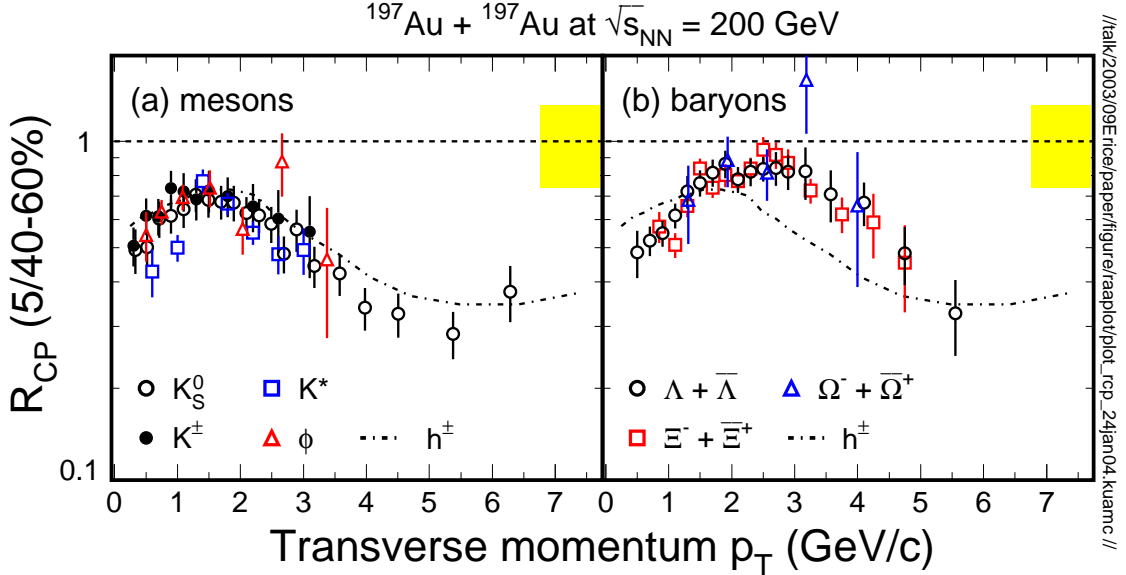

Figure 4 *STAR preliminary results of mid-rapidity R_{CP}, 0-5% over 40-60%, for mesons (a) and Baryons (b). The R_{CP} of charge hadrons is also shown as dot-dashed lines in both plots. The error bars shown include both statistical and systematic errors. The widths of the gray band represent the uncertainties in model calculations of N_{bin}, the number of binary collisions.*

3. Hadron spectra – Bulk properties

In this section, we will discuss the transverse momentum spectra of identified hadrons, including kaons, protons, Ξ and the ϕ meson production mechanism in high energy heavy ion collisions.

The mid-rapidity ($|y| \leq 0.5$) proton and anti-proton transverse mass distributions are shown in Figure 5 for all 8 centrality bins. These data are from the Au+Au collisions at 130 GeV [30]. Here, the transverse mass m_t is given by $m_t = \sqrt{(p_t^2 + m_0^2)}$, with m_0 the rest mass of the proton(anti-proton). It is evident that both proton (left panel) and anti-proton (right panel) distributions become more convex from peripheral to central collisions. This increase with centrality is also reflected in the values of $\langle p_t \rangle$, shown in Figure 6. In order to extract total yields, dN/dy and mean transverse momenta $\langle p_t \rangle$, thermal model fits [31] were applied. These fits simultaneously describe experimental spectra of charged pions [32], kaons [33], protons and anti-protons. The fit-results are shown as dashed lines in Figure 5. The velocity profile $\beta_t(r) = \beta_s(r/R)^{0.5}$ was used in the fit, where R and β_s

are the radius and the surface velocity of the source, respectively. When strong collective flow develops, the transverse mass distributions for heavy mass particles will not have a simple exponential shape at low transverse mass. This effect becomes particularly strong when the temperature is low. The hydrodynamically motivated two parameter fits (T_{fo}, β_t) then become necessary [34]. The increase of $\langle p_t \rangle$ with centrality is indeed reflected in the values of the collective velocity parameter $\langle \beta_t \rangle$, which increase from about $0.41c$ to $0.55c$ from the most peripheral to the most central collisions, respectively.
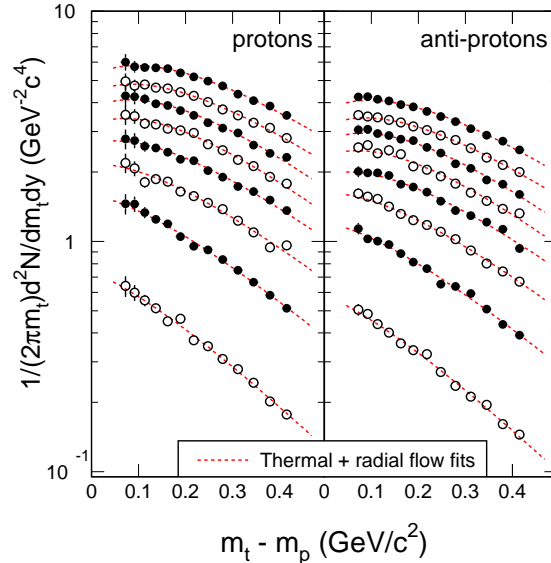

Figure 5 *Mid-rapidity ($|y| \leq 0.5$) proton (left column) and anti-proton (right column) transverse mass distributions for most peripheral (bottom) to most central (top) collisions. Relatively large systematic errors for protons in the low p_t region are due to the background subtraction. The thermal model fit results are shown as dashed lines.*

The top panels of Figure 6 show the $\langle p_t \rangle$ within $|y| \leq 0.5$ for protons (left) and anti-protons (right). The corresponding yields, dN/dy are shown in the bottom panels. The open symbols represent fiducial yields and filled ones show the total yields. The hatched bands indicate the systematic uncertainties in extracting $\langle p_t \rangle$ and dN/dy. The increase of $\langle p_t \rangle$ vs. centrality in the figure implies the development of stronger collective expansion in more central collisions. Results from calculations with RQMD [35], RQMD with re-scattering switched off and HIJING [9,36] are represented by solid, dashed, and dashed-dotted lines, respectively. In the RQMD model [35,37] hadronic re-scattering has been implemented, which leads to the agreement with measurements of the mean transverse momentum. On the other hand, without the re-scattering mechanism, the HIJING model under-predicts the proton(anti-proton) $\langle p_t \rangle$, especially for central collisions. Overall, the model calculations fail to predict the experimental yields consistently throughout the whole centrality range.

As one can see from the bottom panels of Figure 6, the observed mid-rapidity ($|y| \leq 0.5$) proton and anti-proton yields, dN/dy are found to be proportional to the number of charged hadrons. RQMD fails to predict the centrality dependence of the anti-proton yield due to the strong annihilation in hadronic re-scattering, especially in central collisions. Because of the annihilation, RQMD predicts a change in the $\overline{p}/p$ ratio of almost a factor

of two from peripheral to central collisions, which is not consistent with observations [38].

The results from RQMD show that late hadronic re-scatterings build up large values of $\langle p_t \rangle$ and lead to strong annihilation among baryons. In the RQMD calculations the annihilation of initially created anti-protons increases from 20% in peripheral collisions to 50% in the most central collisions. The experimental data exhibit an approximately linear increase in proton and anti-proton yields with the number of negatively charged hadrons (see Figure 6). We may therefore reach the following conclusions: On the one hand, if the annihilation of baryons with anti-baryons increases with centrality, then the centrality dependence of the initial baryon production rate can only be stronger than linear as currently observed. Thus our experimental yields may be inconsistent with the initial baryon production mechanism in the RQMD model. On the other hand, if the initial baryon production is correctly modeled by RQMD, then our measurement indicates a smaller anti-proton loss due to annihilation in the most central collisions. In this case, protons and anti-protons might have inherited collective flow from an earlier stage [39,40] in order to attain the large experimental values of $\langle p_t \rangle$. In order to distinguish different scenarios and possible early stage partonic collectivity at RHIC, a systematic measurement of multi-strange baryons, charmed mesons and particle correlations become necessary.
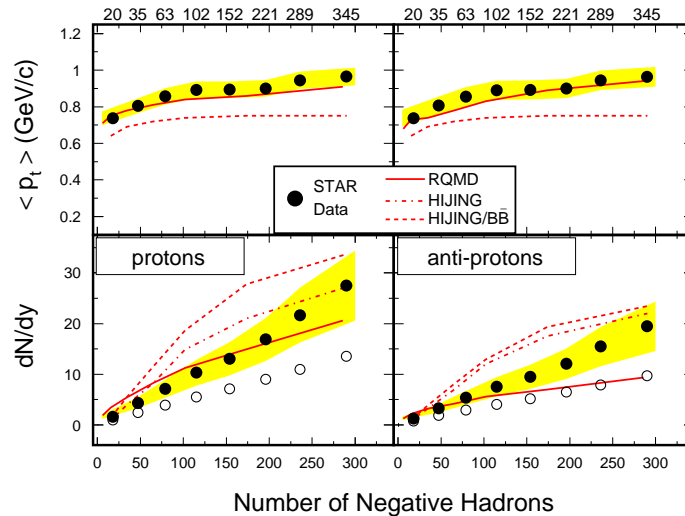

Figure 6 *Mid-rapidity $\langle p_t \rangle$ and dN/dy of proton and anti-proton as a function of the number of negatively charged hadrons. The data are from Au+Au collisions at 130 GeV. Open symbols are fiducial yields and filled ones are total yields. Systematic errors in the integrated yields are shown as hatched areas. Results from RQMD with re-scattering switched off (wø) and HIJING are shown as solid-lines, dashed-lines and dashed-dotted lines respectively. The experimental data and the results from RQMD and HIJING include feed-down from hyperon decay. The number of the participants for each centrality is also shown at the top of the plots.*

Within STAR, the particle identification (PID) based on the TPC dE/dx information becomes very difficult at $p \sim 1$ GeV/c. Other methods like the mixed-event, decay-topology, photon-conversion are also used for PID in STAR. Due to the TPC large acceptance with high efficiency, these methods are very effective and suffer very small

edge effects [41]. In STAR, in addition to the measured stable particles, distributions of $\pi^0, K_S^0, K^*, \rho, \Delta^{\pm}, \phi, \Lambda, \Xi, \Omega, D^{0,\pm}, D^*$ have been measured [24,42–46,26].
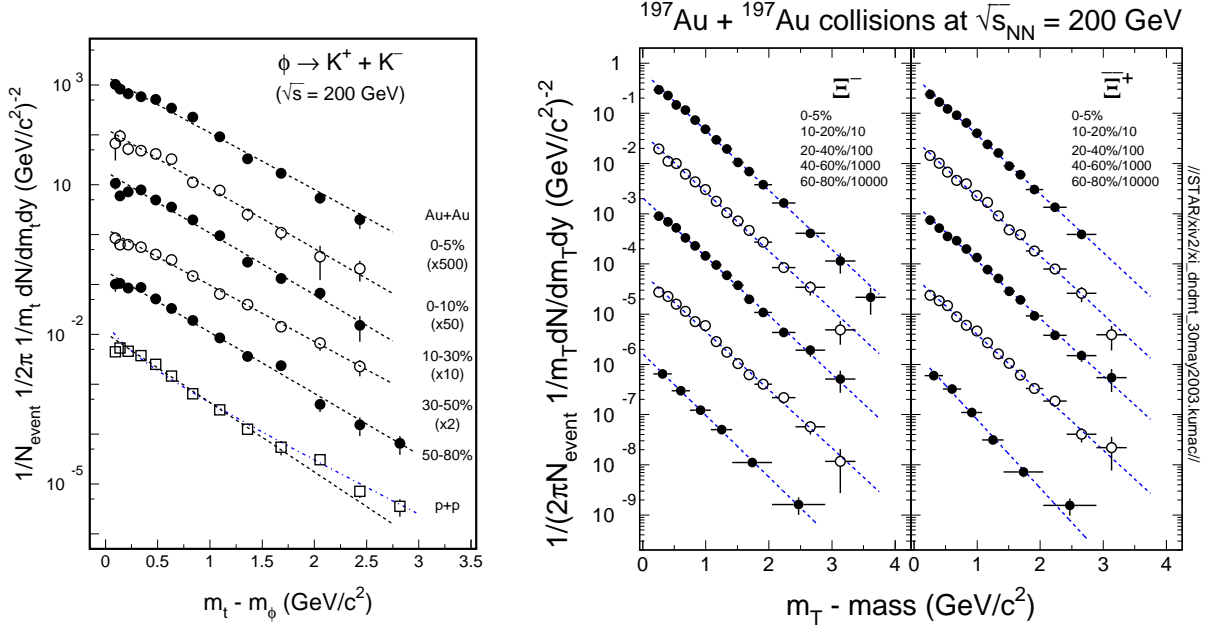

Figure 7 *Left-plot: Mid-rapidity ϕ transverse mass distributions from 200 GeV $Au+Au$ and $p+p$ collisions. Dashed-line represent exponential fits to the data and the dot-dashed-line is the power-law fit to the $p+p$ result; Right-plot: Mid-rapidity Ξ transverse mass distributions from 200 GeV $Au+Au$ collisions. Dashed-lines the exponential fits. All data are preliminary.*

In Figure 7, the ϕ meson (left-plot) and Ξ (right-plot) transverse mass distributions from 200 GeV $Au+Au$ and $p+p$ collisions are shown. Dashed-lines represent exponential fits:

$$f_{exp} = A \cdot e^{-m_T/T}, \tag{3}$$

where A and T are the normalization constant and inverse slope parameter, respectively. In case of the ϕ from $p+p$ collisions, a power-law fit gives a better result:

$$f_p = A \cdot (1 + \frac{p_T}{p_0})^{-n}. \tag{4}$$

Here A is the normalization constant and p_0 and n are free parameters that describe the shape of the distributions. In high energy elementary collisions, mesons are following the power-law type while the baryons are more close to the exponential function [47].

In heavy ion collisions at RHIC, as can be seen in Figure 7, all multi-strange hadron distributions are fit well with the exponential function. In contrast to the distributions of π, K, and protons, the slope parameters of both ϕ and Ξ show little sensitivity to the changing of collision centrality. In Figure 8, the values of ϕ $\langle p_t \rangle$ are compared to that of π, K, and anti-proton [48], see Figure 8, plot (a). The general trend for $\bar{p}$, K^- and π^- is an increase in $\langle p_t \rangle$ as a function of centrality, which is indicative of an

increased transverse radial flow velocity component to these particles' momentum distributions. The ϕ $\langle p_t \rangle$, however, increases from $p + p$ to $Au + Au$, but has no significant centrality dependence in $Au + Au$ collisions. This indicates that the ϕ does not participate in the transverse radial flow as do the $\bar{p}$, K^- and π^-. This is expected, however, if the ϕ decouples early in the collision before transverse radial flow is completely built up. If the ϕ hadronic scattering cross section is much smaller than that of other hadrons, one would not expect the ϕ $\langle p_t \rangle$ distribution to be appreciably affected by any final state hadronic rescatterings. In contrast to these observations, the RQMD predictions of $\langle p_t \rangle$ for kaon, proton and ϕ all increase as functions of centrality [35,49].
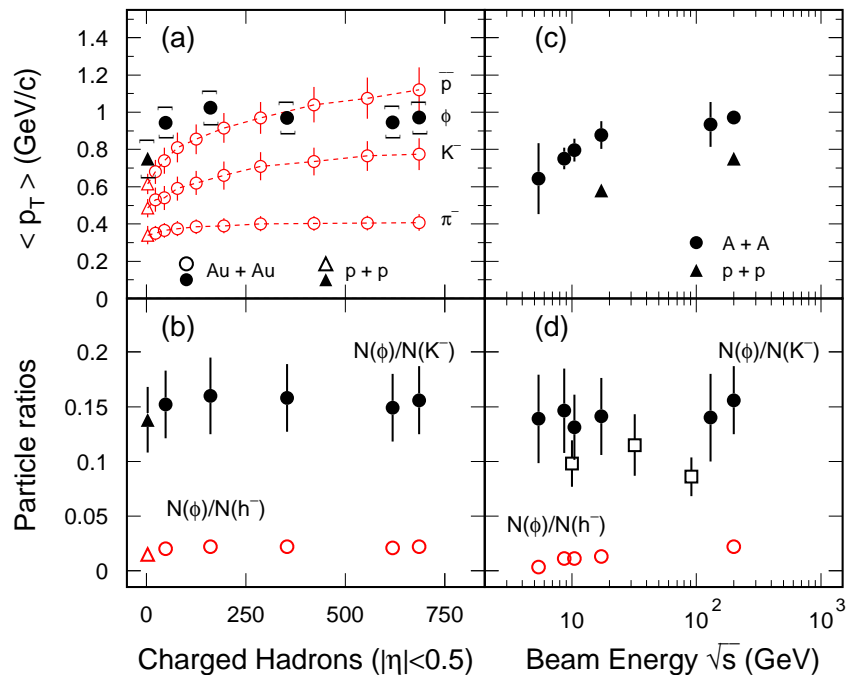

Figure 8 *(a) ϕ $\langle p_t \rangle$ vs. measured number of charged hadrons (N_{ch}) within $|\eta| \leq 0.5$. For comparison, the values of $\langle p_t \rangle$ for negative pions, kaons, and anti-protons are also shown; (b) Ratios of $N(\phi)/N(K^-)$, filled symbols, and $N(\phi)/N(h^-)$, open symbols, vs. N_{ch}; (c) $\langle p_t \rangle$ vs. center of mass beam energy from central nucleus-nucleus (filled circles) and $p + p$ collisions (filled triangles); (d) Ratios of $N(\phi)/N(K^-)$ from central nucleus nucleus collisions, filled circles, and $N(\phi)/N(h^-)$, open circles, vs. center of mass beam energy. Data from e^+e^- (open squares) are also shown. All plots are from mid-rapidity. Both the statistical and systematic errors are shown for the 200 GeV STAR data, while only statistical errors are shown for the energy dependence of the particle ratios.*

The yield ratio ϕ/K^- from this analysis is constant as a function of centrality as shown in Figure 8 (b) and species ($p + p$ or $Au + Au$ for example) Figure 8 (d). In fact, for collisions above the threshold for ϕ production, the ϕ/K^- ratio is essentially independent of system size, e^+e^- to nucleus-nucleus, and energy from a few GeV up to 200 GeV (Figure 8 (d)) [50–55]. This is remarkable, considering that the initial conditions of an

e^+e^- collision are drastically different from $Au + Au$ collisions. This observation perhaps indicates that the ratio is dominated by the hadronization process.

Rescattering models (RQMD[35], UrQMD[56]) assume that about $2/3$ of ϕ mesons come from kaon coalescence in the final state. The centrality dependence of the ϕ/K^- ratio alone provides a serious test of the current rescattering models. In these models, such as UrQMD, rescattering channels for ϕ production includes $K\bar{K}$ and K-Hyperon modes. They predict an increasing ϕ/K^- ratio vs. centrality. These models also predict an increase in $\langle p_t \rangle$ for the proton, kaon, and ϕ of 40 to 50% from peripheral to central collisions. A comparison of the data to these models rules out the kaon coalescence production mechanism for ϕ mesons.
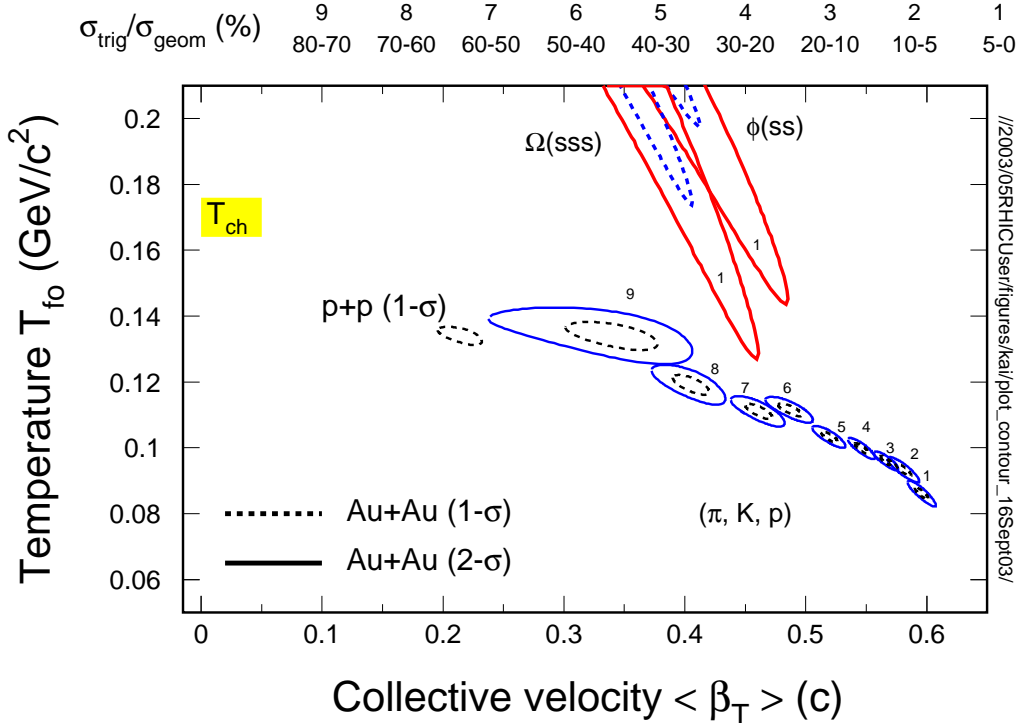

Figure 9 χ^2 *contours, extracted from the thermal+radial flow fits, for copiously produced hadrons π, K and protons and multi-strange hadrons ϕ and Ω. On the top of the plot, the numerical labels indicate the centrality selection. For π, K and protons, 9 centrality bins (from top 5% to 70-80%) were used from the $Au + Au$ collisions. The results from the $p + p$ collisions are also shown. For ϕ and Ω, only the most central results are presented. Dashed- and solid-lines are the 1-σ and 2-σ contours, respectively.*

The different behavior, in the temperature versus collective velocity plane, between the relatively rarely produced multi-strange particles and copiously produced particles π, K and protons is shown in Figure 9. The χ^2 contours are extracted from the thermal + radial flow fits [31] and presented in the temperature-velocity space. The numerical labels indicate the centrality selection. For π, K and protons, 9 centrality bins were used from the $Au + Au$ collisions and $p + p$ collisions [48]. For ϕ and Ω, only the most central results are shown. Dashed- and solid-lines are the 1-σ and 2-σ contours, respectively.

As the collision centrality changes from peripheral to central, for copiously produced hadrons, π, K and protons, the temperature parameter decreases and the velocity parameter increases. At the most central collisions, the velocity becomes as high as 60% of the speed of light. On the other hand, the fit results indicate that the minima for multi-strange hadrons are not sensitive to collisions centrality and they are all close to a temperature of T $\sim$ 180 MeV and the average velocity of $\beta \sim 0.4$.

While thermal freeze-out temperature for π, K and proton is about 100 MeV, the temperature parameter from the multi-strange hadrons is the same as the chemical freeze-out temperature [57–61] extracted from high energy collisions and it is close to the value of the phase transition temperature [2]. Due to relatively small total hadronic cross sections [62,49], multi-strange particles do not participate in the evolution of the system during the hadronic phase. As a result, they de-associate from the system near the hadronization point with $T \sim 170$ MeV and $\beta \sim 0.4$

Alternatively, Broniowski *et al.* assume a single freeze-out. The apparent low freeze-out temperature and large collective velocity for copiously produced particles pion, kaon and protons is explained due to resonance decay [63]. However, it is not clear if this scenario can also explain the resonance data [46] at RHIC.
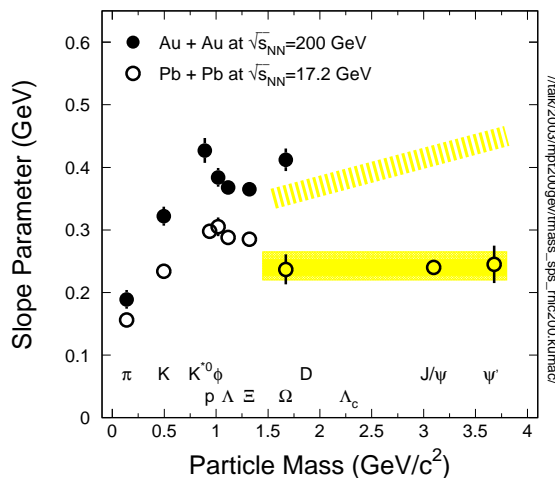

Figure 10 *Slope parameters as a function of hadron mass for Pb+Pb central collisions at SPS (open-circles) and Au+Au central collisions at RHIC (filled-circles). The increase of the hatched band indicating the development of collectivity at high energy nuclear collisions at RHIC.*

Figure 10 shows the slope parameters of identified hadrons as a function of particle mass. At SPS energies (open circles) the multi-strange hadrons do not show an increase as mass increases. At RHIC energy, however, the slope parameters for Ξ and Ω seem to increase with their mass indicating the development of partonic collectivity at RHIC [61]. In order to confirm partonic collectivity, we must study the elliptic flow of multi-strange particle produced at RHIC. That will be discussed in the next section.

4. Elliptic flow v_2 – Evidence of partonic collectivity at RHIC

The particle azimuthal distribution with respect to the reaction plane at a given rapidity window can be deconvoluted by the expansion:

$$\frac{dN}{d\phi} \approx v_0(1 + 2v_1 \cos(\Delta\phi) + 2v_2 \cos(2\Delta\phi)). \tag{5}$$

The first and second Fourier coefficients, v_1 and v_2, are connected to directed flow and elliptic flow, respectively. The coefficient v_0 is a normalization constant and $\Delta\phi$ is defined as the azimuthal angle difference between the particle and the event reaction plane. At a given rapidity the coefficients are: $v_1 = \langle\cos(\Delta\phi)\rangle$ and $v_2 = \langle\cos(2\Delta\phi)\rangle$, commonly noted directed and elliptic flow, respectively. Because the rescattering induced expansion suppresses the spatial anisotropy, the early information of the collision dynamics can be learned through measuring v_1, v_2 and higher order harmonics [64–67].
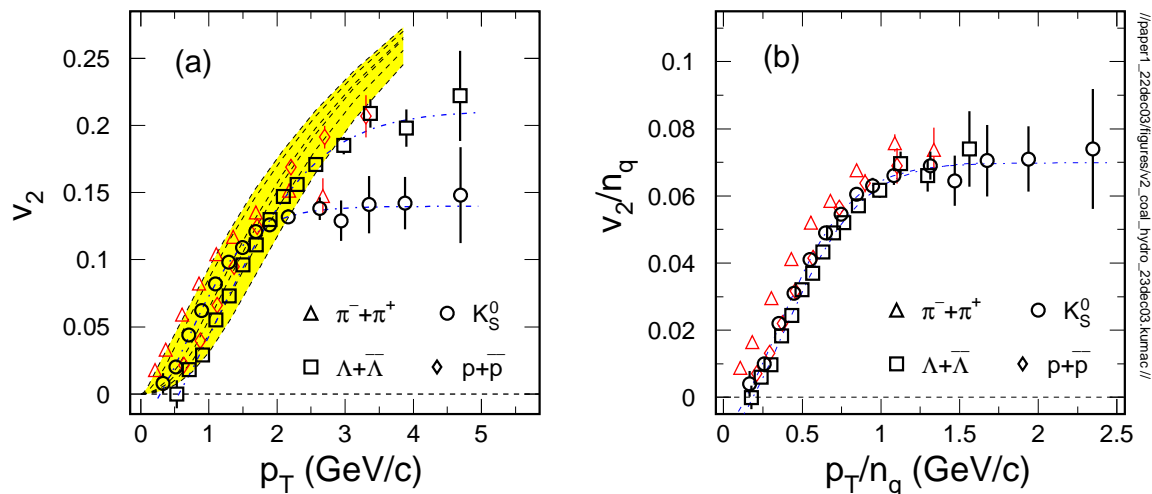

Figure 11 *(a) The $v_2(p_T)$ for π, K_0^S, p, and Λ from minimum bias $Au + Au$ collisions at $\sqrt{s_{\mathrm{NN}}}$ =200 GeV [68]. Respectively, the dashed-lines, from top to bottom, represent the elliptic flow of π, K, p, Λ, Ξ, Ω from hydrodynamic calculations [70]. Dashed-lines are the fits to K_0^S and Λ v_2 distributions. (b) v_2 and p_T scaled by the number of constituent quarks - indicating the collectivity at the partonic stage. Except pions, all hadrons follow the NCQ-scaling.*

The measured elliptic flow v_2 from $Au + Au$ collisions at $\sqrt{s_{\mathrm{NN}}} = 200$ GeV for π, K_0^S, p, Λ are shown in Figure 11 (a). The results of pions and protons are from the PHENIX experiment [68]. Respectively, from top to bottom the dashed-lines represent the elliptic flow of $\pi, K, p, \Lambda, \Xi, \Omega$ from hydrodynamic calculations [70]. At lower p_T, the v_2 results are well reproduced by the hydrodynamic calculations. At higher p_T, v_2 becomes saturated and hydrodynamic results over predict the data. While the baryons saturate at $p_T \geq 3$ GeV/c with $v_2 \sim 0.2$, the mesons' saturation starts earlier at lower values of v_2. According to coalescence approaches [71], after scaling both values of v_2 and p_T with the number of the constituent quarks (NCQ) of the corresponding hadron, all particles should fall onto

14

one single curve. Figure 11(b) shows the scaled v_2. Indeed all particles follow one curve except the pions. This means that there is collectivity developed at the partonic stage.

The measured v_2 distributions are fitted with the equation given as:

$$f_{v_2} = \frac{a}{1 + exp(-(x - b)/c)} - d \qquad (6)$$

where parameters a, b, c and d are fixed from the fit. The fit results to K_S^0 and λ are shown as dot-dashed lines in Figure 11. In the NCQ scaled plot, Figure 11(b), the fit results are also shown. For kaon, proton and lambda, the scaling seems working within $p_T/n_q \leq 2.5$ GeV/c. Pions (open triangles) do not follow the scaling. In high energy collisions, it is well known that a large fraction of hadrons produced through resonance decay. This is particularly true for pions in high energy heavy ion collisions [72,73]. At mid-rapidity, in collisions at RHIC, as high as $\sim 80\%$ of pions are from resonance decays and the dominant sources for pion production are ρ, K^*, K_S^0 and baryon resonances like Λ.

In order to test this idea, we need two basic information on the resonance production. First is their v_2 distributions. Assuming the NCQ-scaling, as demonstrated in Figure 11, one can readily estimate their v_2 distributions via Eq. (1). Secondly one needs to know the relative yields of the resonances. This information is determined from the chemical fits [61] provided the relative yields are fixed at the chemical freeze-out.
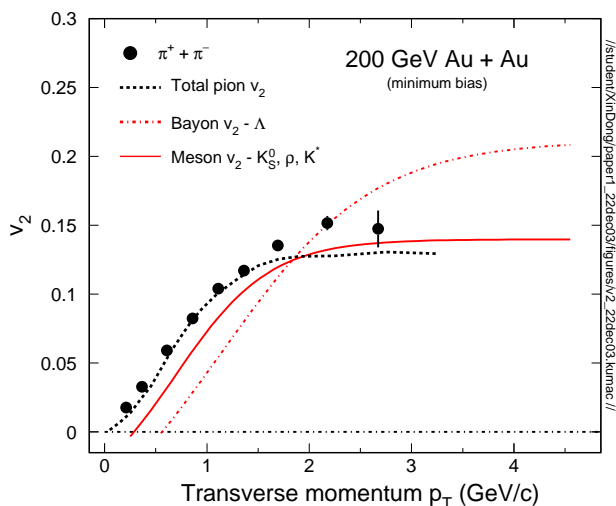

Figure 12 *Resonance decayed pion v_2 (symbols) versus transverse momentum dependence. Dashed line represent the sum of the resonance decay effects. Solid and dot-dashed lines are the v_2 versus p_T curves for mesons and baryons, respectively.*

The simulated result is shown as dashed line in Figure 12. Resonances of ρ, K^*, K_S^0 and Λ are used in this study. The dominant resonance is the ρ-meson because (i) 100% of the ρ decay into pions and (ii) the production cross section is large. The rapidity width of $|y| \leq 0.5$ has been used in the present study and no effect on the final results are seen with wider rapidity windows. It is clear that it fits the pion v_2 well with the resonance decay for $p_T \leq 2$ GeV/c. Due to the relatively small Q-value, the p_T of the decayed pions from ρ, K^* is not much lower than their resonance parents.

In the region $p_T \leq 1$ GeV/c, most of pions are from resonances at $\leq p_T \leq 2$ GeV/c where the values of v_2 are already reach their maximum resulting higher values of v_2 for pions after decaying. Pions from the baryon resonance decay have the narrowest distribution due to large asymmetry in the mass of the decay daughters. As a result, the baryon resonance effect on pion v_2 will be at low $p_T \leq 0.4$ GeV/c while the effect from mesoninc resonance will be dominant at $0.5 \leq p_T$.

When resonance decays are taken into account, the v_2 of primary pions becomes consistent with a NCQ-scaling. The observation of the NCQ-scaling, which can be a natural consequence of hadrons coalescing out of a thermal distribution of partons and the increasing with mass of the multi-strange hadron slope parameters (see Figure 10), indicate that the partonic flow develops at RHIC.
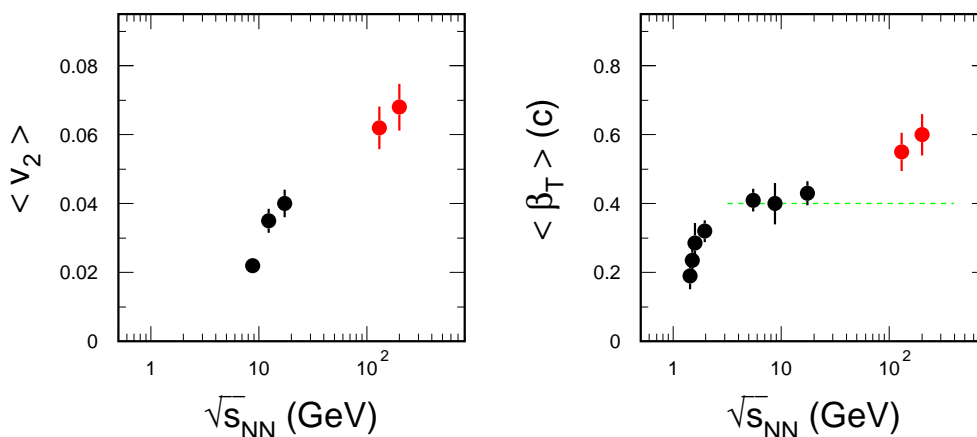

Figure 13 *Collision energy dependence of (Left-panel) the elliptic flow v_2 from minimum biased $Au + Au$ or $Pb + Pb$ interactions; (Right-panel) the radial flow velocity parameter $\langle \beta_T \rangle$ from central $Au + Au$ or $Pb + Pb$ collisions.*

Let us close this section by showing the collision energy dependence of the collective flow observables in Figure 13. The elliptic flow v_2, and the radial flow parameters, β_T, as a function of collision energy. v_2 increases monotonically v_2 implying that more and more early flow develops as the collision energy increases. Assuming that hadronic rescattering effects have already been maximized at the SPS energy ($\sqrt{s_{NN}} \approx 17$ GeV), the net increase in the transverse velocity at RHIC perhaps is due to partonic interactions.

5. Summary and out look

In summary, the suppression of the hadron production at intermediate transverse momentum region ($3 \leq p_T \leq 10$) in central $Au+Au$ and the results from the $d+Au$ collisions provide evidence of early stage, most likely partonic, interactions at RHIC. As a result, the bulk matter created at RHIC demonstrates a stronger collective expansion and larger values of elliptic flow - the development of the partonic collectivity.

In the near future, it is important to quantify the partonic collective flow with high statistics data of v_2 measurements for all hadrons. The results of ϕ v_2 and R_{AB} are specially important because ϕ-meson are unlikely produced through the kaon fusion channel.

These results will provide direct information on the partonic phase.

The next step, perhaps the last necessary measurement needed for the EOS measurement of partonic matter, *i.e.* QGP, is the thermalization for light quarks. According to up to date theory, the QGP temperature is in the order of 0.3 - 0.5 GeV [74,75]. The mass of charm-quark is much heavier than the possible temperature, meaning that thermal excitation of the charm-quark is negligible. Because of their heavy mass, the development of heavy flavor collectivity requires much more parton rescatterings. Hence the measurement of heavy flavor (open-charm) v_2 should be used to probe the equilibrium status of light quarks like u,d, and s at RHIC, in addition to the conventional methods of temperature measurements with thermal photons and di-leptons.

As mentioned in the introduction, the Lattice calculations predicted both phase (hadronic to partonic) and chiral symmetry transitions occur simultaneously [1,2]. Therefore it is necessary to study the hadron properties experimentally. This is possible with the measurements of leptons in several experiments [76,77] at RHIC.

——

REFERENCES

1. H. Satz, Nucl. Phys. **A715**, 3c(2003).
2. F. Karsch, Nucl. Phys. **A698**, 199c(1996).
3. W. Reisdorf and H.G. Ritter, Ann. Rev. Nucl. Part. Sci. **47**, 663(1997).
4. Z. Fodor, Nucl. Phys. **A715**, 319c(2003) and references there in; Z. Fodor and S.D. Katz, Phys. Lett. **B534**, 87(2002).
5. C. Adler *et al.*, (STAR Collaboration), Phys. Rev. Lett. **89**, 202301(2002).
6. J. Adams *et al.*, (STAR Collaboration), Phys. Rev. Lett. **91**, 172302(2003).
7. C. Adler *et al.*, (STAR Collaboration), Phys. Rev. Lett. **90**, 082302(2003).
8. X.N. Wang and M. Gyulassy, Phys. Rev. Lett. **68**, 1480(1992).
9. X.N. Wang, Phys. Rep. **280**, 287(1997).
10. P.L. McGaughey, J.M. Moss, and J.C. Peng, Ann. Rev. Nucl. Part. Sci. **49**, 217(1999).
11. D.M. Alde *et al.*, Phys. Rev. Lett. **64**, 2479(1990).
12. M. Begel, Ph.D Thesis, Rochester University, 1999.
13. K. Adcox *et al.*, (PHENIX Collaboration), Phys. Rev. Lett. **88**, 022301(2002).
14. S.S. Adler *et al.*. (PHENIX Collaboration), sub. to Phys. Rev. **C**, nucl-ex/0308006, August 2003.
15. S.S. Adler *et al.*, (PHENIX Collaboration), Phys. Rev. Lett. **91**, 072301 (2003).
16. C. Adler *et al.*, (STAR Collaboration), Phys. Rev. Lett. **90**, 032301 (2003).
17. C. Adler *et al.*, (STAR Collaboration) Phys. Rev. Lett. **90**, 082302(2003).
18. D. Kharzeev, E. Levin, and L. McLerran, Phys. Lett. **B561**, 93(2003).
19. M. Gyulassy, I. Vitev, X.N. Wang, and B. Zhang, nucl-th/0302077 and references therein.
20. K. Gallmeister, C. Greiner, and Z. Xu, Phys. Rev. **C61**, 044905(2003).

21. S.S. Adler *et al.*, (PHENIX Collaboration), Phys. Rev. Lett. **91**, 072303(2003).

22. I Arsene *et al.*, (BRAHMS Collaboration), Phys. Rev. Lett. **91**, 072305(2003).

23. B.B. Back *et al.*, (PHOBOS Collaboration), Phys. Rev. Lett. **91**, 072302(2003).

24. J. Adams *et al.*, (STAR Collaboration), Phys. Rev. Lett. in print, (2003); nucl-ex/0306007.

25. E. Yamamoto, (STAR Collaboration), Nucl. Phys. **A715**, 466(2003.

26. J. Adams *et al.*, (STAR Collaboration), submitted to Phys. Rev. Lett. July, nucl-ex/0307024, (2003).

27. J.W. Cronin *et al.* Phys. Rev. Lett. **31**, 1426(1973); J.W. Cronin *et al.* Phys. Rev. **D11**, 3105(1975); D. Antreasyan *et al.* Phys. Rev. **D19**, 764(1979).

28. P.B. Straub *et al.* Phys. Rev. Lett. **68**, 452(1992).

29. Enke Wang and Xin-Nian Wang, Phys. Rev. Lett. **87**, 142301(2001).

30. J. Adams *et al.*, (STAR Collaboration), submitted to Phys. Rev. Lett. June, (2003); nucl-ex/0306029.

31. E. Schnedermann, J. Sollfrank, and U. Heinz, Phys. Rev. **C48**, 2462(1993).

32. M. Calderón de la Barca Sánchez, *et al.* (STAR Collaboration), Nucl. Phys. **A698**, 503c(2002); *ibid.* Ph.D. Thesis, Yale University, USA(2001).

33. C. Adler *et al.*, (STAR Collaboration), sub. to Phys. Lett. **B**; nucl-ex/0206008.

34. I. G. Bearden *et al.*, (NA44 Collaboration), Phys. Rev. Lett **78**, 2080(1997); M. Kaneta, Ph.D Thesis, (NA44 Collaboration), March (1999).

35. H. Sorge, Phys. Rev. **C52**, 3291 (1992).

36. S.E. Vance, M. Gyulassy, and X.N. Wang, Phys. Lett. **B443**, 45(1998); S.E. Vance, Nucl. Phys. **A661**, 230c(1999).

37. B. Monreal *et al.*, Phys. Rev. **C60**, R31903(1999); *ibid.* Phys. Rev. **C60**, R51902(1999).

38. C. Adler *et al.*, (STAR Collaboration), Phys. Rev. Lett. **86**, 4778(2001); *ibid.* **87**, 262302(2001).

39. L. McLerran and J. Schaffner-Bielich, Phys. Lett. **B514**, 29(2001).

40. K.H. Ackermann *et al.*, (STAR Collaboration), Phys. Rev. Lett. **86**, 402(2001).

41. M. Anderson *et al.*, Nucl. Instrum. Meth. **A499**, 659(2003).

42. I.J. Johnson *et al.*, (STAR Collaboration), Nucl. Phys. **A715**, 691c(2003).

43. C. Adler *et al.*, (STAR Collaboration), Phys. Rev. Lett. **89**, 092301(2002).

44. C. Adler *et al.*, (STAR Collaboration), Phys. Rev. **C66**, 061901(R)(2002).

45. J. Adams *et al.*, (STAR Collaboration), submitted to Phys. Rev. Lett. July, nucl-ex/0307023, (2003).

46. Zhang-bu Xu, nucl-ex/0307014, (2003).

47. G. Bocquet *et al.* (UA1 Collaboration), Phys. Lett. **B366**, 441(1996).

48. J. Adams, *et al.*, (STAR Collaboration), submitted to Phys. Rev. Lett., Sept. 2003, nucl-ex/0309012.

49. Y. Cheng, F. Liu, Z. Liu, K. Schweda, and N. Xu, Phys. Rev. **C68**, 034901(2003).

50. K. Hagiwara *et al.*, Phys. Rev. **D66**, 010001 (2002) and references within.

51. S.V. Afanasiev *et al.*, (NA49 Collaboration), Phys. Rev. **C66**, 054902 (2002).

52. B.B. Back *et al.*, (E917 Collaboration), nucl-ex/0304017 (2003).

53. S.V. Afanasiev *et al.*, (NA49 Collaboration), Phys. Lett. **B491**, 59 (2000).

54. L. Ahle *et al.*, (E802 Collaboration), Phys. Rev. **C58**, 3523 (1998).

55. K. Adcox *et al.*, (PHENIX Collaboration), Phys. Rev. Lett. **88**, 242301(2002).

56. M. Bleicher *et al.*, J. Phys. G: Nucl Part. Phys. **25**, 1859-1896 (1999) and S. Bass *et al.*, Phys.Rev. **C60**, 021902(1999).

57. P. Braun-Munzinger, J. Stachel, J. Wessels, and N. Xu, Phys. Lett. **B344**, 43(1995); P. Braun-Munzinger, I. Heppe, and J. Stachel, Phys. Lett. **B465**, 15(1999).

58. F. Becattini, M. Gazdzicki, and J. Sollfrank, Eur. Phys. J. **C5**, 143(1998); F. Becattini, Z. Phys. **C69**, 485(1996); F. Becattini and U. Heinz, Z. Phys. **C76**, 269(1997).

59. J. Cleymans and K. Redlich, Phys. Rev. Lett. **81**, 5284(1998).

60. J. Letessier, J. Rafelski, and A. Tounsi, Phys. Lett. **B328**, 499(1994); M. Kaneta *et al.*, (NA44 Collaboration), J. Phys. G: Nucl. Part. Phys. **23**, 1865(1997).

61. N. Xu and K. Masashi, Nucl. Phys. **A698**, 306c(2001).

62. H. van Hecke, H. Sorge, and N. Xu, Phys. Rev. Lett., **81**, 5764(1998).

63. W. Broniowski and W. Floekowski, Phys. Rev. **C65**, 024905(2002); *idib* Phys. Rev. Lett. **87**, 272302(2001).

64. H. Sorge, Phys. Lett. **B402**, 251(1997).

65. J.-Y. Ollitrault, Phys. Rev. **D46**, 229(1992).

66. S. Voloshin, Nucl. Phys. **A715**, 379c(2003).

67. N. Xu and Z. Xu, Nucl. Phys. **A715**, 587c(2003).

68. S.S. Adler *et al.*, (PHENIX Collaboration), Phys. Rev. Lett. in print, (2003); nucl-ex/0305013.

69. J. Adams, *et al.*, (STAR Collaboration) Phys. Rev. Lett., in print, 2003, nucl-ex/0310029.

70. P. Huovinen, P. Kolb, U. Heinz, P.V. Ruuskanen, and S. Voloshin, Phys. Lett. **B503**, 58(2001).

71. Z. Lin and C. Ko, Phys. Rev. Lett. **89**, 202302(2002); R.J. Fries, B. Mueller, C. Nonaka, S.A. Bass, Phys. Rev. Lett. **90**, 202303(2003); D. Molnar and S. Voloshin, Phys. Rev. Lett. **91**, 092301(2003).

72. Zhang-bu Xu, nucl-ex/0307014, (2003).

73. R.J. Fries, B. Mueller, C. Nonaka, S.A. Bass, Phys. Rev. **C68** 044902(2003); C. Nonaka,B. Mueller,M. Asakawa, S.A. Bass, and R.J. Fries, nucl-th/0312081.

74. Edward V. Shuryak, Phys. Lett. **B78**, 150(1978).

75. R. Rapp, Phys. Rev. **C63**, 054907(2001).

76. The PHENIX Collaboration, http://www.phenix.bnl.gov.

77. The STAR Collaboration, http://www.star.bnl.gov.